Validity of asymptotic models for water waves

Wooyoung Choi, James M. Hyman & Yi A. Li*
Theoretical Division and Center for Nonlinear Studies
Los Alamos National Laboratory, Los Alamos, NM 87545

January 18, 2001

Abstract

In order to explore the validity of asymptotic models for water waves, we study interactions of finite amplitude solitary waves of the Euler equations and their approximate models, including the Korteweg-de Vries equation, the Boussinesq equations, and the Green-Naghdi equations. To simulate fully nonlinear surface wave dynamics, we present a new numerical scheme to solve a system of exact one-dimensional evolution equations reduced from the Euler equations. Traveling wave solutions of this new system are compared with those of the asymptotic models and the relationship among the speed, amplitude and mass of solitary waves are examined. Two types of interactions, head-on and overtaking collisions, of two solitary waves are described in detail. ¿From our numerical simulations, we conclude that the Green-Naghdi equations much better describe the dynamics of solitary waves of finite amplitude than the weakly nonlinear asymptotic models.

1 Introduction

We consider the evolution of strongly nonlinear long waves on the free surface in a homogeneous layer of an ideal fluid governed by the Euler equations. Two of important approaches to this problem include solving the Euler equations via numerical methods, and studying much simpler models derived from the original system under different approximations. The objective of this study is to combine the two approaches and explore the validity of various approximate models by systematically comparing numerical solutions of the Euler equations for interactions of finite amplitude solitary waves with those of the approximate models.

*Present address: Dept. of Mathematical Sciences, Stevens Institute of Technology, Hoboken, NJ 07030

Since the full system is often too complicated to analyze directly, it is quite common to work with much simpler models to understand various physical processes of interest. Various model equations have been proposed to approximate the original system under different physical conditions (for example, see Choi, 1995). Under the assumption of small wave amplitude and long wavelength, weakly nonlinear long wave models such as the Korteweg-deVries (KdV) and the Boussinesq equations (Korteweg & de Vries 1895; Boussinesq 1877) have made important contributions to both the physical understanding of nonlinear wave phenomena and the development of mathematical theories (Scott *et al* 1973). However the weakly nonlinear models cease to be valid for strongly nonlinear regime *e.g.* they do not correctly describe the waves of large amplitude. Relaxing the assumption of small amplitude, it has been shown that the higher-order nonlinear long wave models such as the Green-Naghdi (GN) equations (Green & Naughdi 1976) can be also derived from the Euler equations by using an asymptotic expansion method (Choi & Camassa 1999*a*).

A number of numerical methods have been developed to solve the Euler equations. Among them, the most widely used are the Fourier method and the boundary integral method. Expressing the wave profile and the velocity potential as the Fourier series in horizontal space, Fenton & Rienecker (1982) combined the fast Fourier transform with the leap-frog scheme for the time evolution to numerically solve the problem. The boundary integral method is based on parametrizing the free surface using the Lagrangian coordinates and, by applying the Green's theorem, the velocity potential is expressed in terms of a distribution of singularities on the free surface. After the pioneering work by Longuet-Higgins & Cokelet (1976), this method has been further developed by using various types of singularities and discretizations for singular integrals in the sense of Cauchy principal value.

The present numerical method to solve the Euler equations is different from these two methods aforementioned. Combining the conformal mapping of the fluid region of interest to a strip with the Hamiltonian structure of the Euler equations, Dyachenko, Zakharov & Kuznetsov (1996) have derived a closed system of pseudo-differential evolution equations for the free surface elevation and the velocity potential on the parameterized free surface. This idea was further developed and tested by Choi & Camassa (1999*b*) for periodic traveling waves. The new formulation provides a novel way of computing the evolution of fully nonlinear surface waves in the sense that it does not require approximation of complicated singular integrals and it is easy and straightforward to implement by using the fast Fourier transformation.

The paper is organized as follows. In the next section, we present a numerical scheme to solve the new exact evolution equations. In §3, we review the derivation of model equations: the KdV equation, the Boussinesq equations, and the GN equations, and show the relationships between them. In §4, we compare our numerical solutions for solitary waves with those for the models presented in §3. In §5, we study two-solitary wave collisions and and discuss interaction processes in detail.

2 Exact evolution equations

A two-dimensional ideal flow between the free surface at $y = \zeta(x,t)$ and the flat bottom at $y = -h$, is governed by the Euler equations, written in terms of the velocity potential $\Phi(x,y,t)$:

$$\begin{array}{ll} \Phi_{xx} + \Phi_{yy} = 0, & -h < y < \zeta,\ -\infty < x < \infty, \\ \Phi_y = \zeta_t + \Phi_x \zeta_x, & -\infty < x < \infty,\ y = \zeta(x,t) \\ \Phi_t + \frac{1}{2}|\nabla\Phi|^2 + gy = \mathcal{S} + \mathcal{P}_E/\rho, & -\infty < x < \infty,\ y = \zeta(x,t) \\ \Phi_y = 0, & -\infty < x < \infty,\ y = -h \end{array} \tag{2.1}$$

where ρ is the fluid density, $\mathcal{S} = \sigma\zeta_{xx}/(1+\zeta_x^2)^{3/2}$ is the surface tension, and $\mathcal{P}_E(x,t)$ is a known external atmospheric pressure.

Following the work by Dyachenko *et al* (1996) and Choi & Camassa (1999*b*), let $z(\xi,\eta,t) = x(\xi,\eta,t) + iy(\xi,\eta,t)$ be an analytic function in the horizontal strip $-\bar{h} \le \eta \le 0$, where $z - \xi$ is periodic in ξ with the period l, such that z maps the rectangle of $-l/2 \le \xi \le l/2$, $-\bar{h} \le \eta \le 0$ onto the fluid domain. The mapping function is assumed to satisfy $y(\xi,0,t) = \zeta(x(\xi,0,t),t)$ and $y(\xi,-\bar{h},t) = -h$ for any $\xi \in [-l/2, l/2]$. It follows from the Cauchy-Riemann equations that the parametrized functions $x(\xi,\eta,t)$, $y(\xi,\eta,t)$, $\phi(\xi,\eta,t) = \Phi(x(\xi,\eta,t), y(\xi,\eta,t), t)$ and its harmonic conjugate $\psi(\xi,\eta,t)$ are related by Fourier multiplier transforms (Choi & Camassa 1999*b*) in the sense that, if the Fourier series of $y(\xi,0,t)$ and $\psi(\xi,0,t)$ are given by

$$y(\xi,0,t) = a_0 + \sum_{k=1}^{\infty}\big[a_k\cos(2\pi k\xi/l) + b_k\sin(2\pi k\xi/l)\big],$$
$$\psi(\xi,0,t) = \alpha_0 + \sum_{k=1}^{\infty}\big[\alpha_k\cos(2\pi k\xi/l) + \beta_k\sin(2\pi k\xi/l)\big],$$

then, for any $\eta \in [-\bar{h}, 0]$, we have

$$\begin{aligned} y(\xi,\eta,t) &= \frac{a_0+h}{\bar{h}}\eta + a_0 + \sum_{k=1}^{\infty} S_h\big[a_k\cos(2\pi k\xi/l) + b_k\sin(2\pi k\xi/l)\big], \\ \psi(\xi,\eta,t) &= \frac{\alpha_0}{\bar{h}}\eta + \alpha_0 + \sum_{k=1}^{\infty} S_h\big[\alpha_k\cos(2\pi k\xi/l) + \beta_k\sin(2\pi k\xi/l)\big], \\ x(\xi,\eta,t) &= \frac{a_0+h}{\bar{h}}\xi + x_0 + \sum_{k=1}^{\infty} C_h\big[a_k\sin(2\pi k\xi/l) - b_k\cos(2\pi k\xi/l)\big], \\ \phi(\xi,\eta,t) &= \frac{\alpha_0}{\bar{h}}\xi + \phi_0 + \sum_{k=1}^{\infty} C_h\big[\alpha_k\sin(2\pi k\xi/l) - \beta_k\cos(2\pi k\xi/l)\big], \end{aligned} \tag{2.2}$$

for $S_h = \sinh\big[2\pi k\big(\eta+\bar{h}\big)/l\big]/\sinh\big(2\pi k\bar{h}/l\big)$ and $C_h = \cosh\big[2\pi k\big(\eta+\bar{h}\big)/l\big]/\sinh\big(2\pi k\bar{h}/l\big)$. In (2.2), $\bar{h}$ and α_0 are functions of time such that $\bar{h} = a_0 + h$ and $\alpha_0 = c\bar{h}$ for constant c to be fixed from the initial condition. Then x_t and ϕ_t are periodic functions of ξ.

On the free surface at $\eta = 0$, we obtain, from (2.2), the following relations

$$x_\xi = 1 + Ty_\xi\,, \qquad \phi_\xi = c + T\psi_\xi\,,$$

to give

$$x = \xi + x_0 + Ty\,, \qquad \phi = c\xi + \phi_0 + T\psi\,,$$

where x_0 and ϕ_0 are functions of time to be determined and T is the Fourier multiplier operator defined by

$$T\big[y\big] = \sum_{k=1}^{\infty} \coth(2\pi k\bar{h}/l)\,\Big[a_k \sin(2\pi k\xi/l) - b_k \cos(2\pi k\xi/l)\Big]\,,$$

which we call as the T-transform. For deep water ($h \to \infty$), this becomes the Hilbert transformation. By substituting the expressions for x, y, ϕ and ψ at $\eta = 0$ into the boundary conditions at the free surface in (2.1), we obtain the following evolution equations

$$\begin{aligned} x_t &= -x_\xi T\left[\frac{\psi_\xi}{J}\right] + y_\xi\left(\frac{\psi_\xi}{J}\right), \\ y_t &= -x_\xi\left(\frac{\psi_\xi}{J}\right) - y_\xi T\left[\frac{\psi_\xi}{J}\right], \\ \phi_t &+ \phi_\xi T\left[\frac{\psi_\xi}{J}\right] + \frac{1}{2J}\left(\phi_\xi^2 - \psi_\xi^2\right) + gy = \mathcal{S} - \mathcal{P}_E/\rho, \end{aligned} \tag{2.3}$$

for $J = x_\xi^2 + y_\xi^2$ and the surface tension $\mathcal{S} = \sigma(y_{\xi\xi}x_\xi - y_\xi x_{\xi\xi})/J^{3/2}$. These are the exact parametric equations governing the surface waves in water of finite depth. Since x and y are related by the Cauchy-Riemann relationship, it seems to be sufficient to choose one of the first two equations with the third equation in (2.3) to solve the system but we still need all of them in our numerical scheme to determine both $x_0(t)$ and $a_0(t)$ from the first two equations.

To numerically solve the equations (2.3), we use a higher-order adaptive predictor-corrector scheme for time, *i.e.* the Adams-Bashforth scheme as the predictor and the Adams-Moulton method as the corrector. At each time step, we express the solution (x, y, ϕ, ψ) as the discrete Fourier series with respect to variable ξ and use the fast Fourier transform (Staley 1999) to compute the solution, its derivatives and T-transform.

In the absence of surface tension and atmospheric external pressure, the surface wave problem possesses nine one-parameter symmetry groups (Benjamin and Olver 1982), from which eight conserved quantities can be found. In order to check the accuracy of our

numerical scheme, we compute the following three conserved quantities: conservation of mass

$$\int_{-l/2}^{l/2} y(\xi)x_\xi(\xi)\,d\xi,$$

conservation of the horizontal momentum

$$\int_{-l/2}^{l/2} \phi_\xi(\xi)y(\xi)\,d\xi\,,$$

and conservation of energy

$$\int_{-l/2}^{l/2} \big(\phi_\xi(\xi)\psi(\xi) + gy(\xi)^2 x_\xi(\xi)\big)\,d\xi,$$

where we express the conserved quantities using the parametrized formulation defined in the interval $[-l/2, l/2]$. The absolute error of these conserved quantities is usually at the order of 10^{-4} and the relative error is $O(10^{-3})$. To deal with the aliasing due to the full nonlinearity of the problem and numerical errors, we have introduced artificial damping terms into the three equations in (2.3), such as $\nu\,\triangle\xi\, x_{\xi\xi}$, $\nu\,\triangle\xi\, y_{\xi\xi}$ and $\nu\,\triangle\xi\,\phi_{\xi\xi}$, respectively, where $\triangle\xi$ is the spatial step size satisfying $|\triangle\xi| \le 0.12$ and ν is usually chosen in the range between 0.01 and 0.05.

3 Approximate model equations

We consider the model equations for nonlinear long waves in shallow water: the KdV, Boussinesq and GN equations. Here we briefly sketch the derivation by assuming the typical wavelength l is much greater than the water depth h and check the domain of validity of these models.

By substituting $x = lX$, $y = h(Y-1)$, $t = lT/c_0$, $\zeta = h(H-1)$, $\Phi = c_0 l\varphi + c_0^2 t$ and $c_0^2 = gh$ into the water wave equations (2.1) with $\mathcal{S} = \mathcal{P}_E = 0$, we obtain the following dimensionless equations

$$\begin{array}{ll}
\epsilon^2\varphi_{XX} + \varphi_{YY} = 0, & 0 < Y < H,\\
\epsilon^2\varphi_T + \frac{1}{2}(\epsilon^2\varphi_X^2 + \varphi_Y^2) + \epsilon^2 H = 0, & Y = H,\\
\epsilon^2 H_T + \epsilon^2 H_X\varphi_X = \varphi_Y, & Y = H,\\
\varphi_Y = 0, & Y = 0\,,
\end{array}$$

where $\epsilon = h/l$. For small $\epsilon \ll 1$ for long waves, the velocity potential φ, satisfying the Laplace equation and the bottom boundary condition at $Y = 0$, takes the asymptotic expansion of

$$\varphi(X,Y,T) = \sum_{k=0}^{\infty} \frac{(-1)^k \epsilon^{2k} Y^{2k}}{(2k)!} \frac{\partial^{2k} f(X,T)}{\partial X^{2k}}\,. \tag{3.1}$$

Substituting the expansion for φ in (3.1) into the free surface boundary conditions at $Y = H$ yields the following equations for H and $w \equiv f_x$

$$\begin{aligned} H_T + (Hw)_X &= \frac{\epsilon^2}{6}(H^3 w_{XX})_X + O(\epsilon^4), \\ w_T + ww_X + H_X &= \frac{\epsilon^2}{3}\Big[H^2(w_{XT} + ww_{XX} - w_X^2)\Big]_X + O(\epsilon^4)\,. \end{aligned} \tag{3.2}$$

By using $\varphi_X = w - \epsilon^2 H^2 w_{XX}/2 + O(\epsilon^4)$, the depth-mean horizontal velocity u can be found as

$$u = \frac{1}{H}\int_0^H \varphi_X dY = w - \frac{\epsilon^2 H^2}{6} w_{XX} + O(\epsilon^4)\,, \tag{3.3}$$

and the system (3.2) can be rewritten, in terms of H and u, as

$$\begin{aligned} H_T + (Hu)_X &= 0, \\ u_T + uu_X + H_X &= \frac{\epsilon^2}{3H}\Big[H^3\big(u_{XT} + uu_{XX} - u_X^2\big)\Big]_X + O(\epsilon^4)\,, \end{aligned} \tag{3.4}$$

where we have used, from (3.3), $w = u + \epsilon^2 H^2 u_{XX}/6 + O(\epsilon^4)$. System (3.4) was originally derived by Green & Naghdi (1976) by using the so-called 'direct-sheet' theory but here we show the same system can be derived by an asymptotic expansion method. The method used here to derive the GN equations is analogous to that of Whitham (1974) for the Boussinesq equations and an alternative can be found in Choi & Camassa (1999*a*). Notice that the first equation in the above system is exact, while the second equation from conservation of momentum contains an error of $O(\epsilon^4)$. Since we have imposed no assumption on wave amplitude, the GN equations should behave as good as the Euler equations even for large amplitude waves as long as the long-wave approximation is valid. When we use the horizontal velocity defined at a certain depth instead of the depth mean velocity u in (3.4), we have other forms of equations, (for example, the system by Wei *et al* 1995), which are all asymptotically equivalent to (3.4).

Substituting $H = 1 + \alpha\tilde{\zeta}$ and $u = \alpha\tilde{u}$ for $\alpha = a/h$ into the GN equations (3.4) leads, after dropping $O(\alpha\epsilon^2)$ for weakly nonlinear waves, to the Boussinesq equations:

$$\begin{aligned} \tilde{\zeta}_T + \Big[(1 + \alpha\tilde{\zeta})\tilde{u}\Big]_X &= 0, \\ \tilde{u}_T + \alpha\tilde{u}\tilde{u}_X + \tilde{\zeta}_X &= \frac{\epsilon^2}{3}\tilde{u}_{XXT}. \end{aligned} \tag{3.5}$$

The KdV equation can be derived from the Boussinesq system (3.5) by the assumption of uni-directional waves as shown by Whitham (1974).

In dimensional variables, we can rewrite the GN equations (3.4) as

$$\begin{aligned} &\eta_t + (u\eta)_x = 0, \qquad \eta = h + \zeta\,, \\ &u_t + uu_x + g\eta_x = \frac{1}{3\eta}\left[\eta^2 \frac{d}{dt}(\eta u_x)\right]_x\,, \end{aligned} \tag{3.6}$$

where we have used $d(\eta u_x)/dt = (\eta u_x)_t + u(\eta u_x)_x$. We can also rewrite, in dimensional forms, the Boussinesq equations (3.5) as

$$\begin{aligned} &\zeta_t + \Big[(h+\zeta)u\Big]_x = 0, \\ &u_t + uu_x + g\,\zeta_x = \frac{h^2}{3}\,u_{xxt}\,, \end{aligned} \tag{3.7}$$

and the KdV equation as

$$\zeta_t + c_0\,\zeta_x + \frac{3c_0}{2h}\,\zeta\zeta_x + \frac{c_0 h^2}{6}\,\zeta_{xxx} = 0\,, \tag{3.8}$$

where $c_0 = \sqrt{gh}$.

4 Solitary wave solutions

Here we compare solitary waves of the Euler equations with those of the three model equations considered in the preceding section. While we have to find solitary wave solutions numerically for the Euler and Boussinesq equations, we have explicit solutions for the KdV and GN equations given by

$$\zeta_{KdV} = \frac{2h(c-c_0)}{c_0}\,\mathrm{sech}^2\,\frac{\sqrt{3(c-c_0)}\,(x-ct)}{\sqrt{2c_0}\,h},$$

$$\zeta_{GN} = \frac{c^2-c_0^2}{g}\,\mathrm{sech}^2\,\frac{\sqrt{3(c^2-c_0^2)}\,(x-ct)}{2ch},$$

respectively, for given wave speed c.

4.1 Numerical methods

The existence of solitary waves and their properties have been studied extensively. By using the KdV scaling, Friedrichs & Hyers (1954) and Beale (1977) proved the existence of solitary waves in the weakly nonlinear regime where the Froude number $F = c/\sqrt{gh}$ is greater than but close to one and the solitary waves of the KdV equation approximate those of the Euler equations. Amick & Toland (1981) later showed the existence of solitary

waves as the limit of periodic waves even beyond the weakly nonlinear regime. Based on their results, we numerically find periodic waves of long wavelength as approximations to solitary waves of the Euler equations.

We look for travelling waves of the form

$$x = \xi + \tilde{x}(\xi - ct), \quad y = y(\xi - ct), \quad \phi = \delta(\xi - ct) + \tilde{\phi}(\xi - ct), \quad \psi = \psi(\xi - ct),$$

where $\tilde{x}(= Ty)$, y, ψ and $\tilde{\phi}$ are periodic functions of $s = \xi - ct$ with the period l and δ is a constant to be determined. Here we assume that y and $\tilde{\phi}$ satisfy the boundary condition $y\big(l/2\big) = \tilde{\phi}_\xi\big(l/2\big) + \delta = 0$, and y is even and symmetric with respect to $s = 0$. As $l \to \infty$, y converges to a solitary wave decaying to zero at infinity (Amick & Toland 1981). Substituting the travelling waves into the kinematic equation $y_t x_\xi - x_t y_\xi = -\psi_\xi$ (Choi & Camassa 1999*b*), we obtain $cy_s = \psi_s$. Then by using the fact that $\tilde{x}$ and ϕ are harmonic conjugates of y and ψ, respectively, we have that $\phi_s(s) = c\big(\tilde{x}_s(s) - \tilde{x}_s\big(l/2\big)\big)$, *i.e.* $\delta = -c\tilde{x}_s\big(l/2\big)$. Substituting these relations into the third equation of (2.3) under the condition that the surface tension $\mathcal{S}$ and the external pressure $\mathcal{P}_E$ are negligible, we obtain the equation for the free surface at $\eta = 0$

$$x_\xi^2 + y_\xi^2 = \frac{x_s^2\big(l/2\big)}{1 - 2gy/c^2}\,,$$

which can be reduced to, after substituting $s = \bar{h}\xi$, $x = \bar{h}\hat{x}$, $\eta = \bar{h}\hat{\eta}$ and $y = \bar{h}\hat{y}$, the following dimensionless equation

$$\hat{x}_\xi^2 + \hat{y}_\xi^2 = \frac{\hat{x}_\xi^2\big(l/2\big)}{1 - 2g\bar{h}\hat{y}/c^2} \quad \text{at } \eta = 0\,. \tag{4.1}$$

For simplicity, we will drop the accent ˆ. Because the Euler equations have a one-parameter scaling symmetry group $(\lambda x, \lambda y, \lambda^{\frac{1}{2}} t, \lambda^{\frac{3}{2}}\phi)$ (Benjamin & Olver 1982) for any $\lambda > 0$, without loss of generality, we set $\bar{h} = 1$ throughout our numerical scheme described below.

Let w and θ be real-valued functions such that $z_\xi = x_\xi + iy_\xi = e^{w+i\theta}$ and, since z_ξ is an analytic function of $\xi + i\eta$, w and θ satisfy the Cauchy-Riemann equations. After using the KdV scaling (Friedrichs & Hyers 1954) $\xi^* = a\xi$, $\theta^* = a^{-3}\theta$ and $w^* = a^{-2}w$, the equation for the free surface given by (4.1) can be rewritten as

$$w_\xi = \frac{1}{a^3} e^{a^2\left(3w - 2w(l/2) - 1\right)} \sin a^3\theta \quad \text{at } \eta = 0\,, \tag{4.2}$$

where $e^{a^2} = c^2/\big(g\bar{h}\big)$ and we have dropped the asterisks again for simplicity. ¿From the Cauchy-Riemann relations, the exponent in (4.2) at $\eta = 0$ can be found as

$$3w - 2w(l/2) = 3T_a[\theta] - 2T_a[\theta(l/2)] + < w > \equiv M_a[\theta]\,, \tag{4.3}$$

where $T_a[\theta]$ is the scaled T-transform, in complex form, given by

$$T_a[\theta] = -ia \sum_{k\neq 0} \coth(2\pi ak/l)\, c_k e^{2\pi ik\xi/l}\,,$$

and $< w >$ is the average value of w over its period defined by

$$< w >= -\frac{1}{a^2} \log\left[\frac{1}{l}\int_0^l e^{a^2 T_a \theta} \cos(a^3\theta) d\xi\right]\,.$$

By using (4.3), equation (4.2) can be written in the following form

$$f[\theta] \equiv \theta - (G-I)^{-1}\left[\frac{1}{a^3} e^{a^2\left(M_a[\theta]-1\right)} \sin(a^3\theta) - \theta\right] = 0\,, \tag{4.4}$$

where the operator $G[\theta]$ is defined by

$$G[\theta] = a \sum_{k\neq 0} kl \coth(2\pi ak/l)\, c_k e^{2\pi ik\xi/l}\,.$$

In order to solve (4.4) by using the Newton's method, we replace θ by $\theta_n + v_n$, where θ_n is the result from the previous iteration and v_n is the correction, and we linearize (4.4) with respect to v_n to have $f_\theta[\theta_n]\, v_n = -f[\theta_n]$, where f_θ is the functional derivative of f with respect to θ, given by

$$f_\theta[\theta_n]\, v_n \equiv v_n - (G-I)^{-1}\left[\frac{1}{a} e^{a^2\left(M_a[\theta_n]-1\right)} \sin(a^3\theta_n)\, \frac{\delta M_a}{\delta\theta_n} + e^{a^2\left(M_a[\theta_n]-1\right)} \cos(a^3\theta_n) - 1\right] v_n\,.$$

After we compute f_θ modulus its kernel, still denoted by f_θ, as an N×N matrix using the Fast Fourier Transform for N Fourier modes, we solve $v_n = -f_\theta^{-1}[\theta_n]\, f(\theta_n)$ iteratively until v_n is small enough.

Based on the fact that travelling waves of the KdV equation are close approximations to those of the Euler equations for small amplitude waves (Friedrichs & Hyers 1954; Beale 1977), we use cnoidal wave solutions of the KdV equation as the initial guess to find traveling wave solutions of (4.2) for sufficiently small $a > 0$. Starting from the weakly nonlinear regime, we gradually increase the parameter a (or, equivalently, increasing the speed c), and use solutions for smaller waves as new initial guesses to compute higher amplitude waves as a fixed point problem. In the weakly nonlinear regime, it takes only six iterations for this scheme to reduce the error to $\sup|\theta_{n+1} - \theta_n| < 10^{-13}$ and $\sup|f(\theta_n)| < 10^{-13}$.

By using the method described here, we are able to compute solitary waves of the Euler equations with the Froude number up to $F = 1.27$. Beyond $F = 1.27$, the numerical computation of solitary waves shows high frequency disturbances due to the sharp steepening of wave slope and requires us to increase the number of Fourier modes to reduce numerical errors. Since it is not our objective to compute the highest solitary wave which is known to have the discontinuity of wave slope, we allow the largest number of Fourier modes to be $N = 2^{11}$, beyond which the computation is too expensive.

4.2 Numerical results

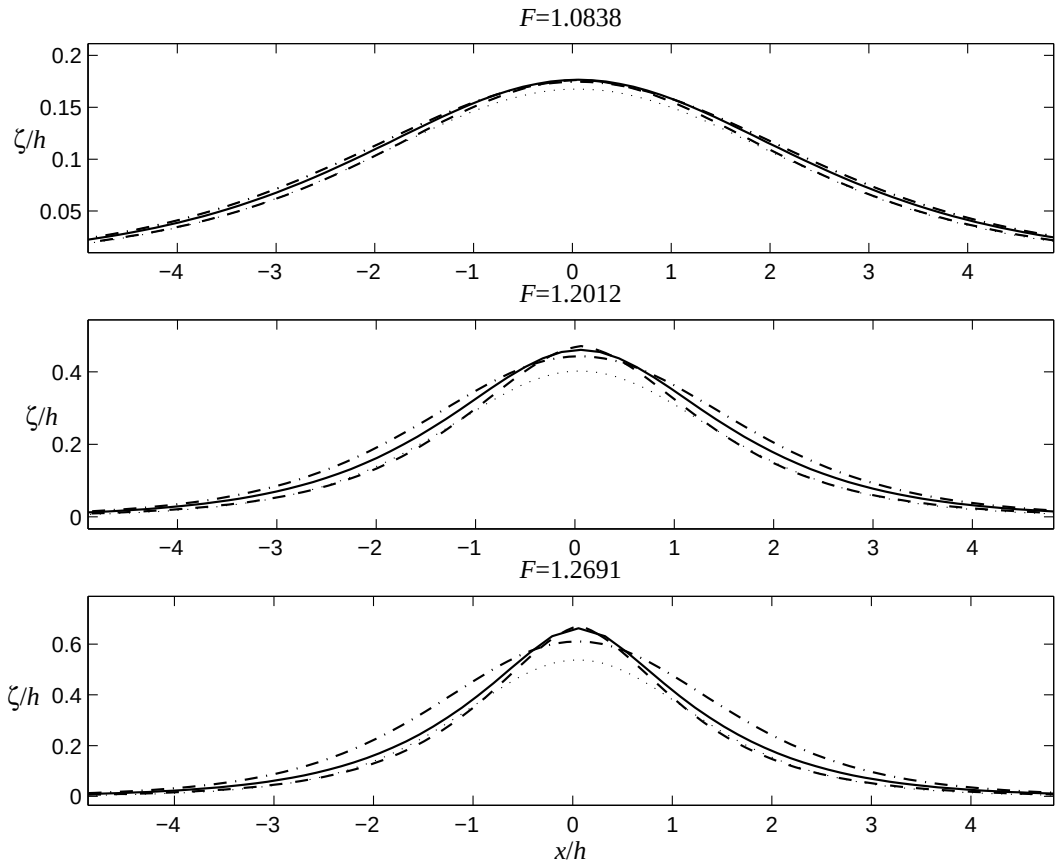

Figure 1: Comparison of solitary wave profiles at the Froude numbers of F =1.0838, 1.2012 and 1.2691; Euler (solid curve), GN (dash-dotted curve), Boussinesq (dashed curve), and KdV (dotted curve).

In figure 1, we compare wave profiles of various models for three different Froude numbers $F = c/\sqrt{gh}$ =1.0838, 1.2012, 1.2691. When the Froude number F is close to 1, say $1 < F \leq 1.1$, solitary wave solutions of the KdV, Boussinesq and GN Equations are very close to those of the Euler equations, as expected. However, as F further increases, solitary waves of the KdV equation start to deviate from those of the Euler equations and, in particular, the wave amplitude is too small, implying the KdV solitary waves are moving too fast for given wave amplitude. For the GN and Boussinesq equations, it is really difficult to tell which model is better than the other by just comparing wave profiles; see wave profiles for $F = 1.2012$ and $F = 1.2691$. The Boussinesq equations seem to have solitary wave profiles closer to the Euler equations in terms of their width. For higher Froude numbers, solitary waves of the GN equations are a little too wide compared with

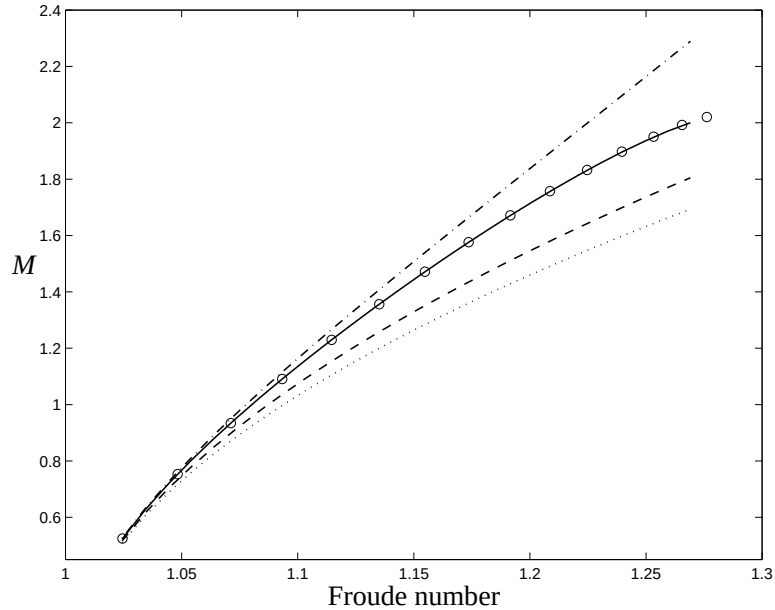

Figure 2: Froude number F versus mass of solitary wave M; Euler (solid curve), GN (dash-dotted curve), Boussinesq (dashed curve), KdV (dotted curve) and Longuet-Higgins & Fenton (circle). The GN equations show much better agreement with the Euler equations than the weakly nonlinear models.

those of the Euler equations.

To make more quantitative comparisons, we measure the scaled mass of solitary waves defined by $M = \int_{\mathbb{R}} \eta dx/h^2$ and the scaled wave amplitude a/h for varying Froude number. In order to verify our numerical solutions for the Euler equations, we also compare our solutions with those by Longuet-Higgins (1974) and Longuet-Higgins & Fenton (1974). As shown in figures 2 and 3, our computations of the dimensionless mass M and amplitude a/h for the Euler equations differ from Longuet-Higgins and Fenton's data only by 0.16% and 0.35%, respectively, and this excellent agreement validates our numerical solutions.

As shown in figure 2, for the Froude number close to 1 ($1 \leq F < 1.1$), the mass of solitary wave of the three model equations agrees well with that of the Euler equations. However, as F continues to increase ($1.1 < F < 1.2$), the weakly nonlinear models such as the KdV and Boussinesq equations cease to be valid, while the strongly nonlinear long wave model (GN) shows much better agreement as long as the mass is concerned. For waves of the Froude number equal to 1.2 or higher, solitary wave solutions from the GN equations are also as poor as other models. Recalling that no assumption on wave amplitude has been imposed in the derivation, the wider range of validity of the GN equations can be easily understood but it still remains to be explained why the GN equations are no longer valid beyond the Froude number around 1.2. At this point, it is worth mentioning that the Froude number for the maximum wave is known to be

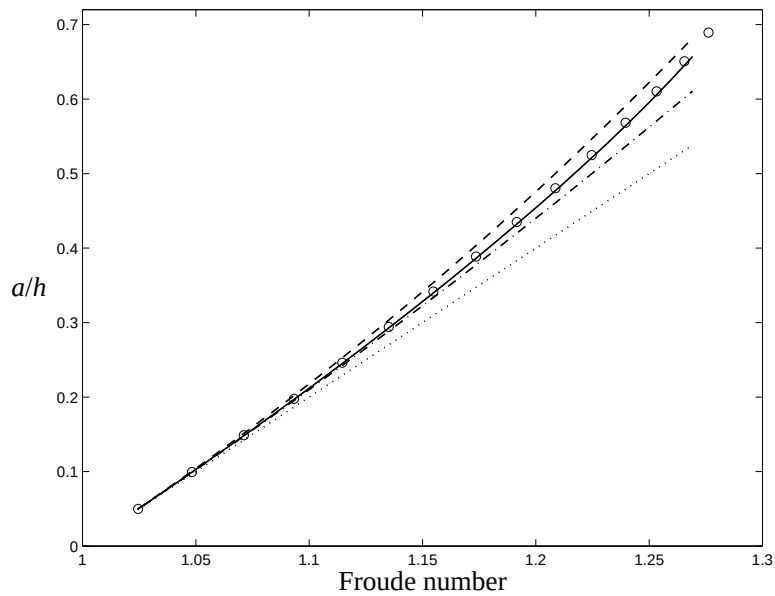

Figure 3: Froude number F versus wave amplitude a/h; Euler (solid curve), GN (dash-dotted curve), Boussinesq (dashed curve), KdV (dotted curve) and Longuet-Higgins & Fenton (circle). Notice that the KdV solitary wave of given wave amplitude is moving too fast.

$F = 1.286$ (Longuet-Higgins & Fentons 1974). As the Froude number approaches this value, the wave slope becomes steeper and the discontinuity in slope finally forms. In this case the long wave approximation to derive any shallow water models is no longer valid and this is why the GN solitary waves of large amplitude near the maximum height differ from the Euler solitary waves. For a system of two fluids, Choi & Camassa (1999a) studied the coupled GN equations describing strongly nonlinear long waves at the interface. At the maximum wave amplitude, instead of having the slope discontinuity, internal solitary wave was shown to become a front varying smoothly from one level to another. Therefore, contrary to the case of surface gravity waves, the coupled GN equations for internal gravity waves are valid even for very large solitary waves.

As shown in figure 3, for given Froude numbers, the wave amplitude of the KdV equation is much smaller than that of the Euler equations, while the GN equations well predict the wave amplitude for $F < 1.2$. Another weakly nonlinear model, the Boussinesq equations, seems to be much better than the KdV equation but it still over-predicts wave amplitude for the whole range of Froude number. In conclusion, based on the comparison between solitary wave solutions of different models, the GN equations show better agreement with the Euler equations than the weakly nonlinear models.

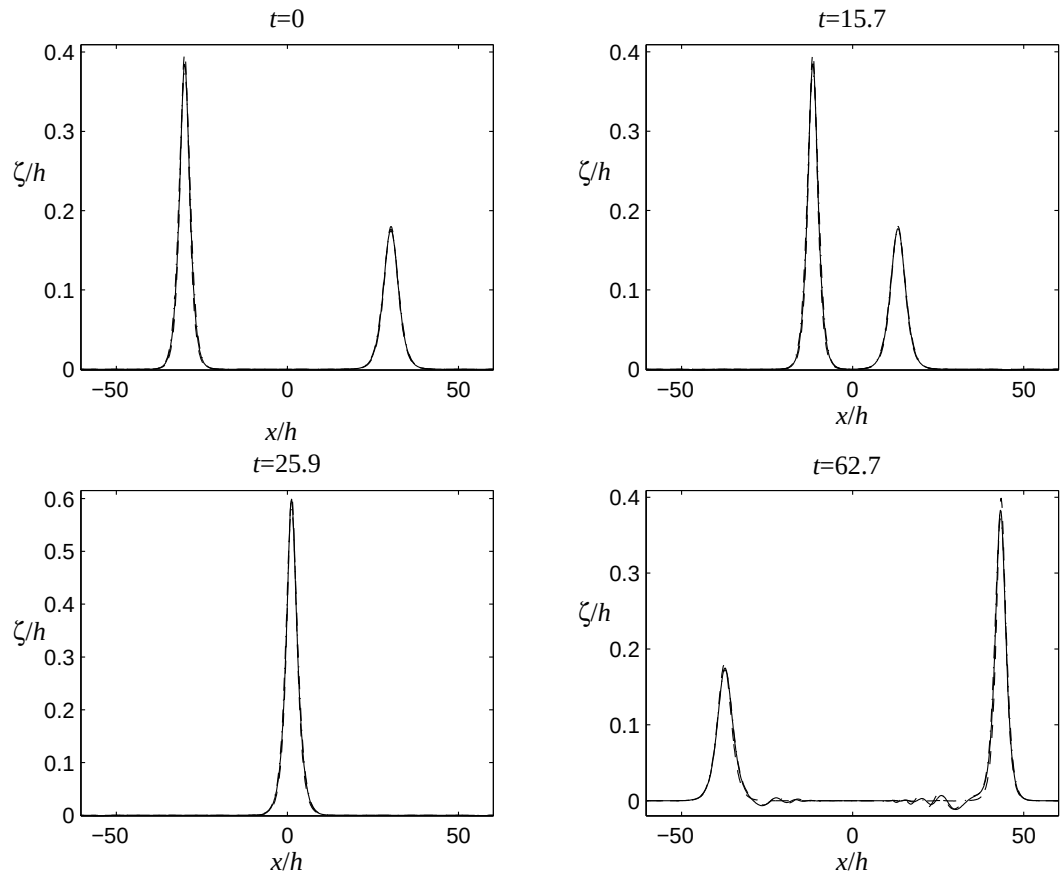

Figure 4: Head-on collision of two-solitary waves of the Euler equations (solid curve), the GN Equations (dash-dotted curve) and the Boussinesq Equations (dashed curve), respectively, with the Froude numbers of $F = 1.084$ and $F = 1.172$.

5 Interaction of two solitary waves

So far we have considered only steady, or time-independent, solutions and we will investigate the dynamical properties of solitary waves of different models in this section. The interaction processes between two solitary waves are examined in detail for both head-on and overtaking collisions. Throughout this section, time t is non-dimensionalized by h/c_0.

For the case of head-on collision, we superpose two different solitary waves propagating in the opposite directions. The Froude numbers of two solitary waves in figures 4 are $F = 1.172$ and $F = 1.084$. In order to match wave speeds, we choose different wave amplitudes for solitary waves of different models: initially, the amplitudes of the larger waves are $A_E/h = 0.3847$, $A_G/h = 0.3727$ and $A_B/h = 0.3991$ and those of the smaller waves are $a_e/h = 0.1765$, $a_g/h = 0.1744$ and $a_b/h = 0.1801$ for the Euler, GN and Boussinesq equations, respectively. Notice that the amplitudes of the larger waves are

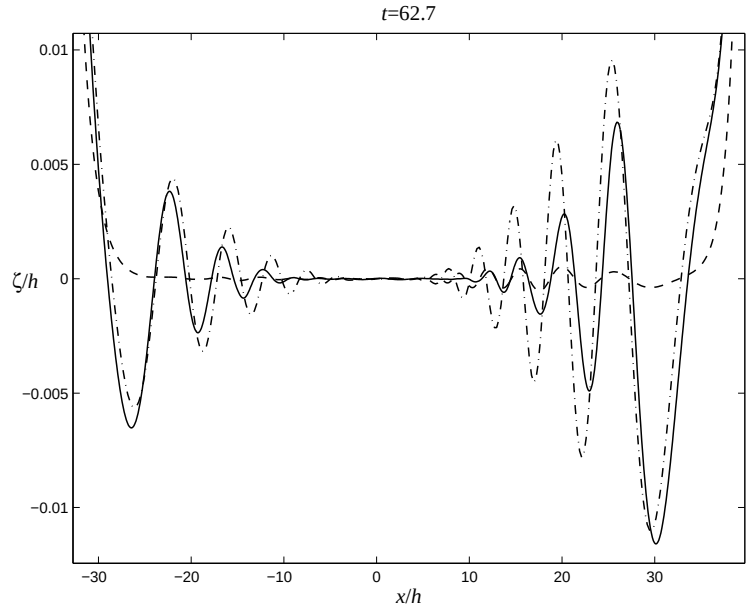

Figure 5: Trailing tails after the head-on collision shown in figure 4 at $t = 62.7$; Euler (solid curve), GN (dash-dotted curve) and Boussinesq (dashed curve). Notice that the GN equations well-capture small trailing waves after head-on collision.

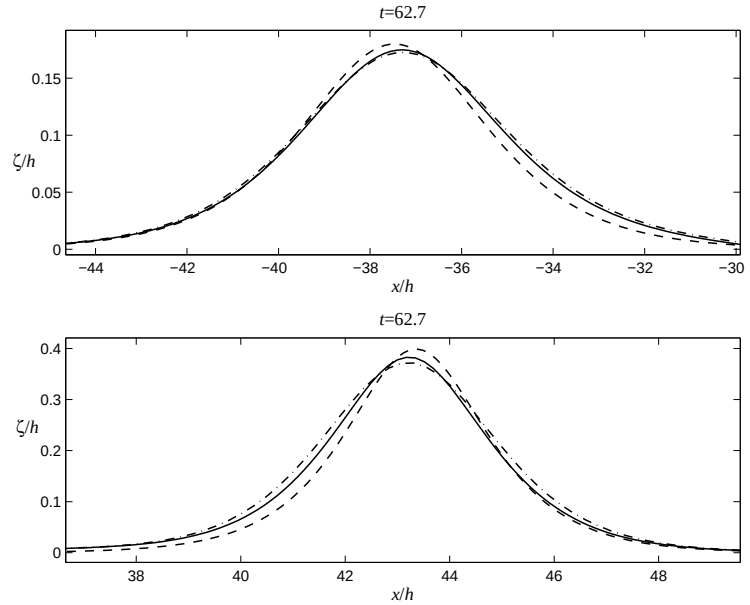

Figure 6: Final wave profiles for $F = 1.084$ and $F = 1.172$ after the head-on collision shown in figure 4; Euler (solid curve), GN (dash-dotted curve) and Boussinesq (dashed curve). After the head-on collision, the GN solitary waves are in phase with the Euler solitary waves, while the Boussinesq equations underpredict the phase shift.

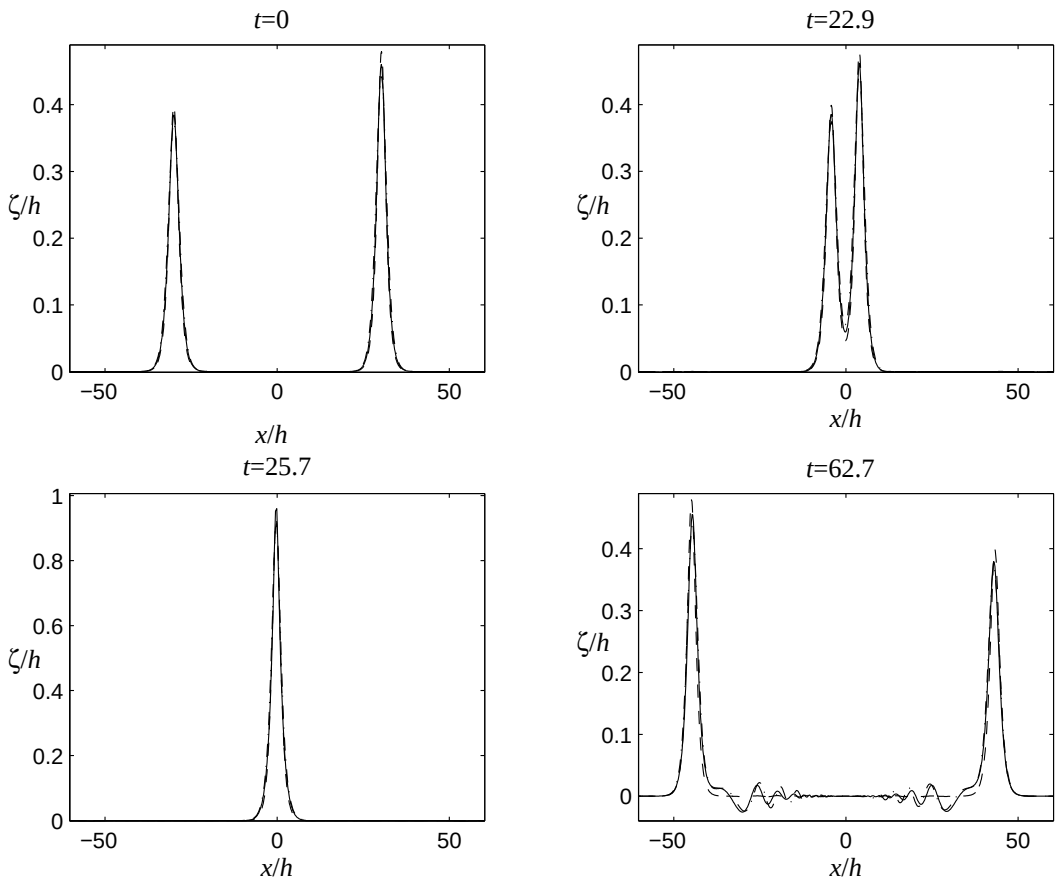

Figure 7: Head-on collision of two-solitary waves of the Euler equations (solid curve), the GN equations (dash-dotted curve) and Boussinesq equations (dashed curve), respectively, with the Froude numbers $F = 1.172$ and $F = 1.201$.

beyond the weakly nonlinear regime. As shown in figure 4, two solitary waves merge and form a single peak at $t = 25.9$ with amplitudes of $A_E/h = 0.5991$, $A_G/h = 0.5802$ and $A_B/h = 0.6052$. The resultant height of the peak is always greater than the sum of two wave amplitudes. They all shed off dispersive waves behind them after the collision and the amplitudes of both waves slightly decrease. At $t = 62.7$, the larger waves have amplitudes of $A_E/h = 0.3828$, $A_G/h = 0.3717$ and $A_B/h = 0.3989$, the smaller waves have amplitudes of $a_e/h = 0.1748$, $a_g/h = 0.1725$ and $a_b/h = 0.1800$. The comparison of dispersive tails after collision is shown in figure 5 and this shows that the GN equations maintain a higher degree of accuracy to approximate the Euler equations than the Boussinesq equations. It is surprising that this approximate model well captures small structures like trailing waves in terms of both phase and amplitude. It is well-known that both waves after the head-on collision are retarded from their own pathlines and this phase shift is the salient feature of nonlinear interaction. The decay of kinetic energy by the retardation upon merging is

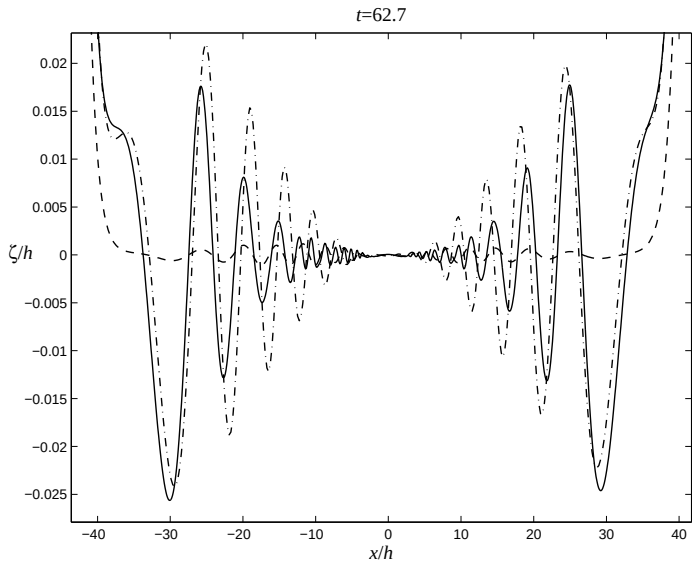

Figure 8: Trailing tails after the head-on collision shown in figure 7 at $t = 62.7$; Euler (solid curve), GN (dash-dotted curve) and Boussinesq (dashed curve).

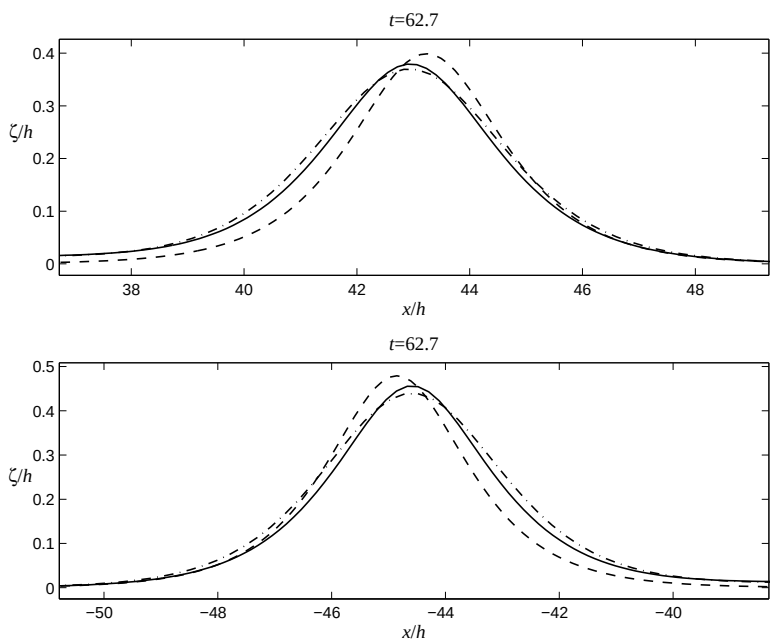

Figure 9: Final wave profiles for $F = 1.172$ and $F = 1.201$ in the head-on collision shown in figure 7; Euler (solid curve), GN (dash-dotted curve) and Boussinesq (dashed curve).

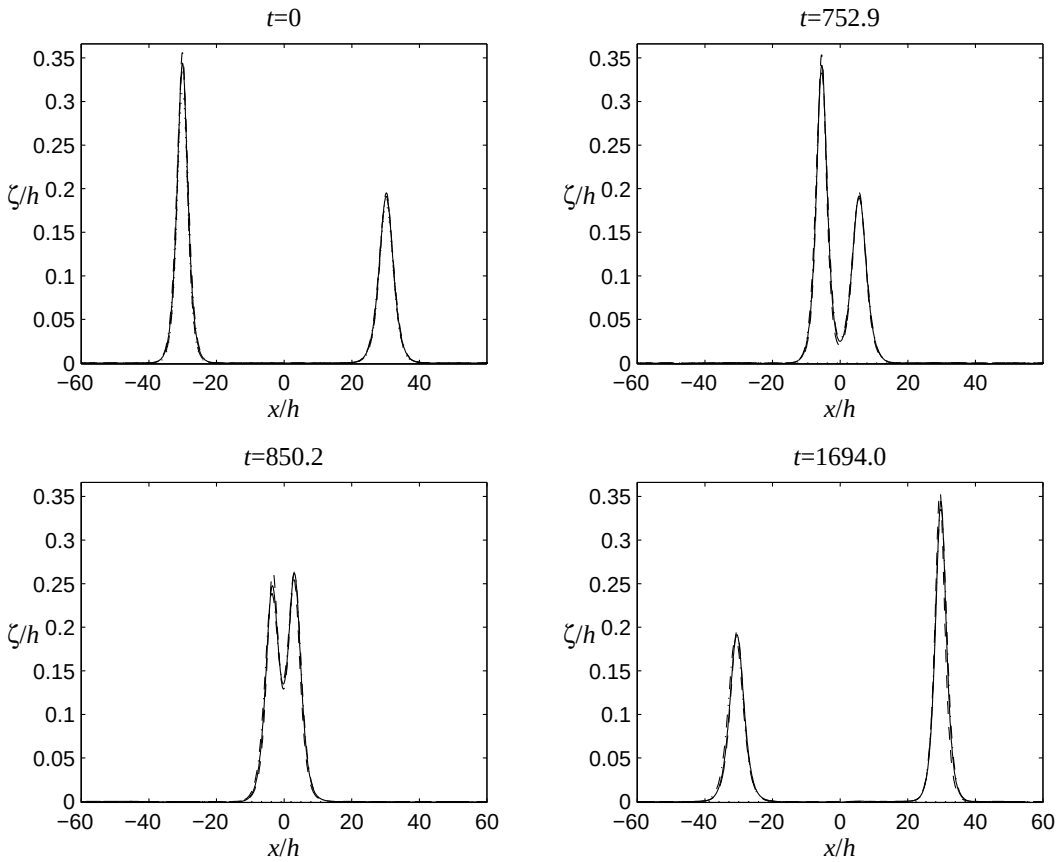

Figure 10: Overtaking collision of two solitary waves of the Euler equations (solid curve), the GN equations (dash-dotted curve), the Boussinesq equations (dashed curve) and the KdV equation (dotted curve), respectively, with $F = 1.156$ and $F = 1.0904$. Unlike the head-on collision, all solitary waves radiate much less trailing tails after their interactions.

compensated by the increase of potential energy, or the increase of the peak height (Wu 1995). ¿From the weakly nonlinear analysis (Wu 1995), the phase shift of one wave is known to be proportional to the square root of amplitude of the other wave, more precisely $\Delta x/h = (\text{amplitude}/3)^{1/2}$. This phase shift is too small to accurately measure from our numerical solutions but the finite amplitude effect on the phase shift can be identified from the relative positions of different solitary waves. As shown in figure 6, the weakly nonlinear model (Boussinesq equations) underpredicts the phase shift after the collision, while the GN equations are in good agreement in phase with the Euler equations. This property becomes more noticeable when we conduct similar simulations for even higher amplitude waves, as shown in figures 7, 8 and 9. In this simulation, we choose two solitary waves whose Froude numbers are $F = 1.172$ and $F = 1.201$. The similar observations for dispersive tails and phase shifts can be made as before. ¿From our numerical results,

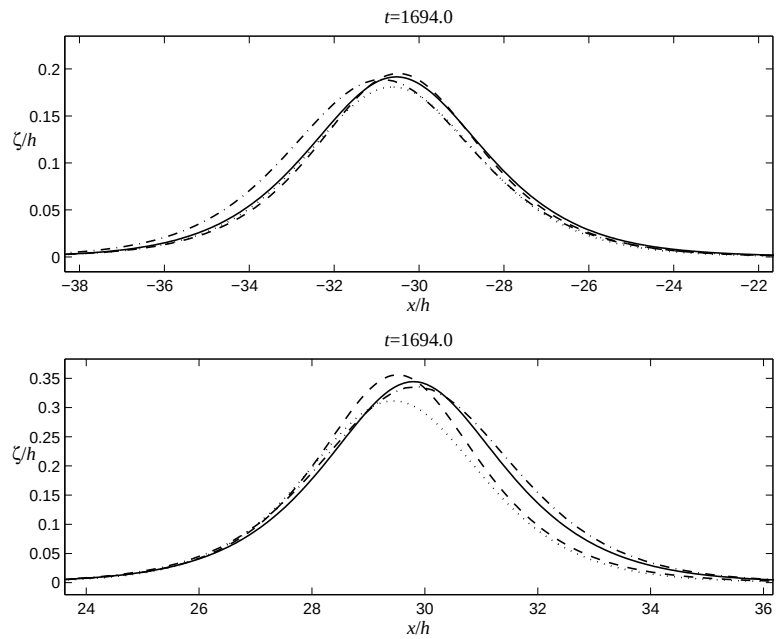

Figure 11: Comparison of solitary wave profiles with $F = 1.156$ and $F = 1.0904$ after the overtaking collision, shown in figure 10; Euler (solid curve), GN (dash-dotted curve), Boussinesq (dashed curve) and the KdV equation (dotted curve), respectively.

we can conclude that the strong nonlinearity in the GN and Euler equations induces the larger phase shift. ¿From the two simulations for head-on collision, we can see that solitary waves of these three systems are not solitons, *i.e.* they do not maintain the same shape after interactions, and dispersive tails become larger as solitary wave amplitudes increase.

Next we study overtaking-collision of two solitary waves of the KdV equation and other three bi-directional equations. Figure 10 shows the overtaking collision between two solitary waves with the Froude numbers of $F = 1.156$ and $F = 1.09$ in a frame moving with the speed $F = 1.123$. Initially, the amplitudes of the larger waves are $A_K/h = 0.3114$, $A_E/h = 0.3441$, $A_G/h = 0.3356$ and $A_B/h = 0.3561$, and the amplitude of the smaller waves are $a_k/h = 0.1808$, $a_e/h = 0.1911$, $a_g/h = 0.1889$ and $a_b/h = 0.1952$ for the KdV, Euler, GN and Boussinesq equations, respectively. Unlike the head-on collision case, all solitary waves radiate much less trailing tails after their interactions. The wave amplitude remains almost unchanged after interaction except the KdV solitons, which exactly preserve their entities except phase shifts. It is interesting to observe that, during the interaction of two solitary waves shown in figure 10, they never merge into a single peak. Instead there is always a gap between their peaks and their amplitudes gradually change in time: the larger amplitude decreases while the smaller amplitude is increasing. This phenomenon was explained earlier by Wu (1995) for the Boussinesq equations, who showed that there exists a critical ratio between two wave amplitudes, which is 3. Above

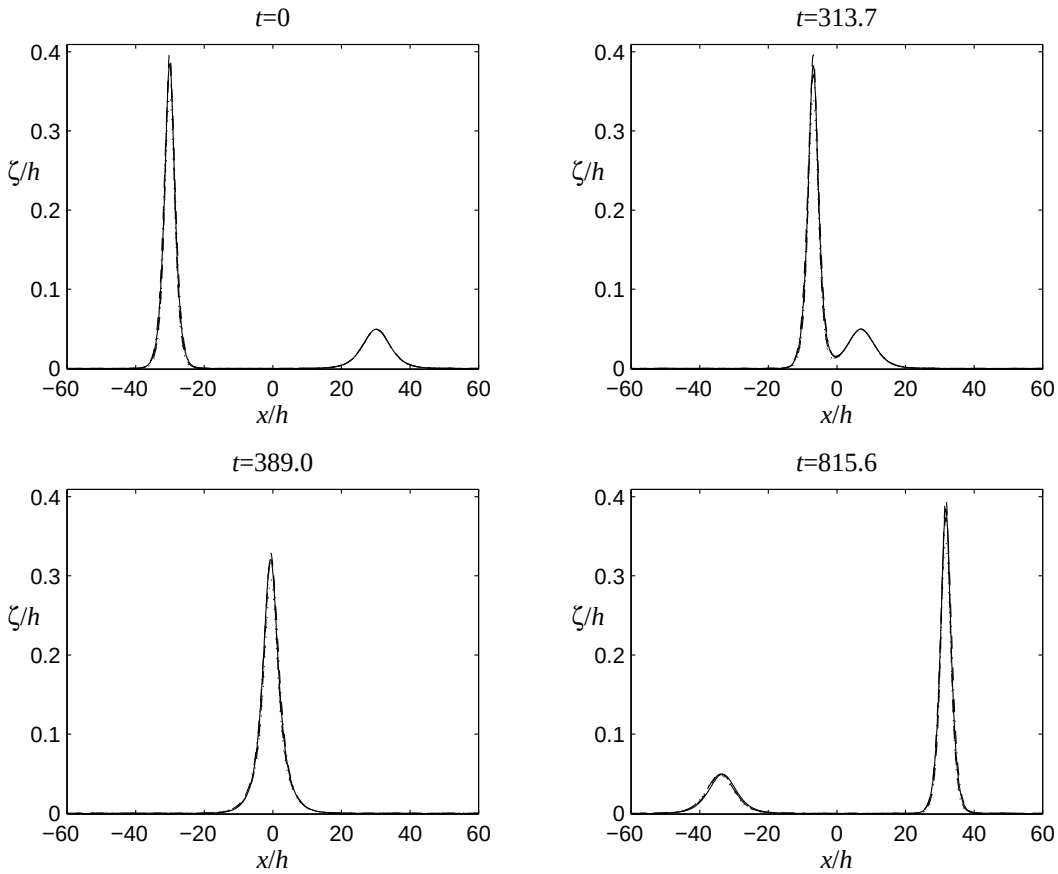

Figure 12: Overtaking collision of two solitary waves of the Euler equations (solid curve), the GN Equations (dash-dotted curve), the Boussinesq Equations (dashed curve) and the KdV equation (dotted curve), respectively, with the Froude numbers $F = 1.172$ and $F = 1.024$.

this ratio, two solitary waves merge together to form a single peak; two wave crests remain separated throughout interactions below this ratio. The amplitude ratio in the simulation shown in figure 10 is less than 3 and two solitary waves never merge. It is also known that a larger solitary wave overtaking a smaller one experiences a forward phase shift, while the smaller one suffers a backward phase shift. The height at the center of mass is known to be the difference of two wave amplitudes. In figure 11, it is shown that the larger waves of the GN and Euler equations move slightly more forward implying larger phase shifts than those of the weakly nonlinear models, while the smaller waves of all models are almost in phase.

In figure 12, we show two solitary-wave interactions with the Froude numbers $F = 1.172$ and $F = 1.024$. The simulation was performed in a frame moving with the speed equal to $F = 1.098$. Their amplitude ratio is about 7.8. In this case the larger wave merges

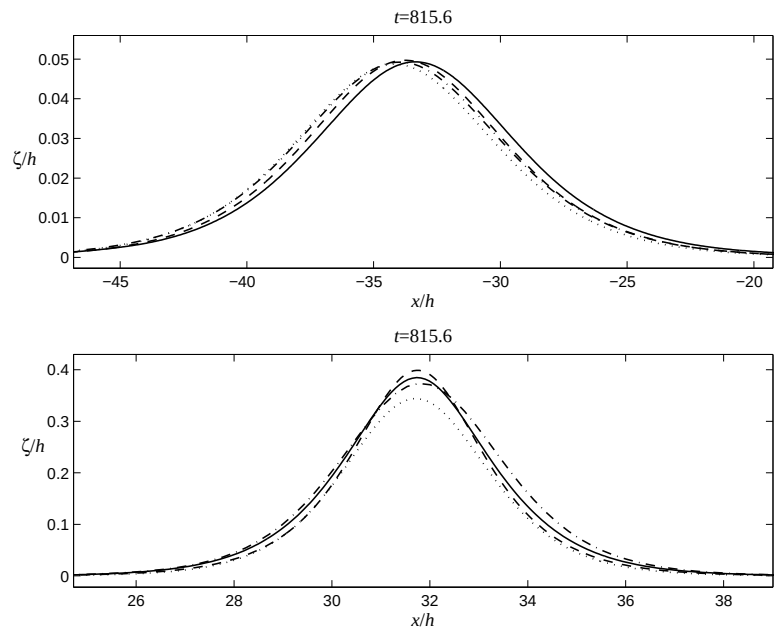

Figure 13: Comparison of solitary wave profiles of the Froude numbers $F = 1.172$ and $F = 1.024$ after the overtaking collision shown in figure 12; Euler (solid curve), GN (dash-dotted curve), Boussinesq (dashed curve) and the KdV equation (dotted curve), respectively. Notice that, for overtaking collision, all three model equations well approximate the Euler equations.

with the smaller wave to form a single peak during the interaction. The amplitude of the peak is about $A_E/h = 0.3208$, smaller than that of the larger wave, $A_E/h = 0.3847$, as the weakly nonlinear theory predicts. As shown in figure 13, both larger and smaller solitary waves of all models are almost in phase after overtaking collision, except a slightly larger phase shift in the smaller solitary wave of the Euler equations. In both simulations for the overtaking case, we observe that solitary waves of the four systems have slightly different phase shift after interactions, and all three model equations well approximate the Euler equations.

6 Conclusion

It is a great challenge to solve the Euler equations for free surface problems due to their highly nonlinear character that the shape of the boundary is unknown *a priori*. As demonstrated in the simulations of two solitary wave interactions, the system of exact one-dimensional evolution equations (2.3) has provided a relatively easy numerical formulation compared with the boundary integral method. As mentioned in §2, we have monitored three conserved quantities, mass, horizontal momentum and energy, of the Eu-

ler equations in our simulations. The relative error of these conserved quantities is about 0.43% even for long simulations over dimensionless time $t = 1700$ and our numerical scheme is very reliable. Although we have considered only solitary waves, the new formulation for surface gravity-capillary waves introduced in §2 is still valid to periodic waves of arbitrary wavelength, and the scheme has a capacity to simulate long time behavior of wave propagations numerically.

Comparing interaction processes between two solitary waves, we have demonstrated that the correct dynamical properties of solitary waves can be captured only by the strongly nonlinear model such as the GN equations, in particular, for the interaction of bi-directional waves. Steady solitary wave solutions of the weakly nonlinear Boussinesq equations in §4.2 seems to be a good approximation to exact solutions of the Euler equations but their dynamics are quite different from strongly nonlinear models such as the GN or Euler equations, as shown in §5. This may be explained by the fact that the GN equations are a higher order nonlinear approximation to the Euler equations than the other weakly nonlinear models shown in §3.

¿From our numerical simulations, we conclude that the GN equations possess a wider range of validity than any weakly nonlinear asymptotic models considered in this paper. We believe that this system can be successfully applied to more realistic physical problems in the coastal area with uneven bottom topography.

References

[1] C. J. Amick and J. F. Toland, *On periodic water-waves and their convergence to solitary waves in the long-wave limit*, Phil. Trans. Royal Soc. London A **303** (1981), 633–669.

[2] C. J. Amick and J. F. Toland, *On solitary water-waves of finite amplitude*, Arch. Rational Mech. Anal. **76** (1981), 9–95.

[3] T. Beale, *The existence of solitary waves*, Comm. Pure Appl. Math **30** (1977), 373–389.

[4] T. B. Benjamin and P. J. Olver, *Hamiltonian structure, symmetries and conservation laws for water waves*, J. Fluid Mech **125** (1982), 137–185.

[5] J. Boussinesq, *Essai sur la théorie des eaux courants*, Mem. prés. div. Sav. Acad. Sci. Inst. Fr. **23** (1877), 1–680.

[6] W. Choi, *Nonlinear evolution equation for two-dimensional surface waves in a fluid of finite depth*, J. Fluid Mech **295** (1995), 381–394.

[7] W. Choi and R. Camassa, *Fully nonlinear internal waves in a two-fluid system*, J. Fluid Mech **396** (1999*a*), 1–36.

[8] W. Choi and R. Camassa, *Exact evolution equations for surface waves*, J. Eng. Mech **125** (1999*b*), 756–760.

[9] A. L. Dyachenko, V. E. Zakharov, and E. A. Kuznetsov, *Nonlinear dynamics of the free surface of an ideal fluid*, Plasma Physics Report **22** (1996), 916–928.

[10] J. D. Fenton and M. M. Rienecker, *A Fourier method for solving nonlinear water-wave problems: application to solitary-wave interactions*, J. Fluid Mech **118** (1982), 411–443.

[11] K. O. Friedrichs and D. H. Hyers, *The existence of solitary waves*, Comm. Pure Appl. Math. **7** (1954), 517–550.

[12] A. E. Green and P. M. Naughdi, *Derivation of equations for wave propagation in water of variable depth*, J. Fluid Mech **78** (1976), 237–246.

[13] D. J. Korteweg and G. de Vries, *On the change of form of long waves advancing in a rectangular canal, and on a new type of long stationary waves*, Phil. Mag **39** (1895), 422–443.

[14] M. S. Longuet-Higgins, *On the mass, momentum, energy and circulation of a solitary wave*, Proc. R. Soc. Lond **A. 337** (1974), 1–13.

[15] M. S. Longuet-Higgins and E. .D. Cokelet, *The deformation of steep surface waves on water I. A numerical method of computation*, Proc. R. Soc. Lond **A. 350** (1976), 1–26.

[16] M. S. Longuet-Higgins and J. D. Fentons, *On the mass, momentum, energy and circulation of a solitary wave. II*, Proc. R. Soc. Lond **A. 340** (1974), 471–493.

[17] A. C. Scott, F. Y. F. Chu, and D. W. McLaughlin, *The soliton: a new concept in applied science*, Proc. IEEE **61** (1973), 1443–1483.

[18] M. Staley, *DFTmod, modules for discrete Fourier transforms and filters*, Technical report, the Los Alamos National Laboratory, 1999.

[19] G. Wei, J. T. Kirby, S. T. Grilli, and R. Subramanya, *A fully nonlinear Boussinesq Model for surface waves. 1. Highly nonlinear unsteady waves*, J. Fluid Mech. **294** (1995), 71–92.

[20] G. .B. Whitham, *Linear and nonlinear waves*, John Wiley and Sons, 1974.

[21] T. Y. Wu, *Bidirectional soliton street*, Acta Mechanica Sinica **11** (1995), 289–306.